Coexistence of unipolar and bipolar modes in Ag/ZnO/Pt resistive switching memory with oxygen-vacancy and metal-Ag filaments*

Han-Lu Ma(马寒露), Zhong-Qiang Wang(王中强)†, Hai-Yang Xu(徐海阳)‡, Lei Zhang(张磊), Xiao-Ning Zhao(赵晓宁), Man-Shu Han(韩曼舒), Jian-Gang Ma(马剑钢), and Yi-Chun Liu(刘益春)

Center for Advanced Optoelectronic Functional Materials Research and Key Laboratory for Ultra Violet (UV) Light-Emitting Materials and Technology of Ministry of Education, Northeast Normal University, Changchun 130024, *China*

(Received 15 March 2016; revised manuscript received 5 August 2016; published online 25 October 2016)

In this study, the unipolar resistive switching (URS) and bipolar resistive switching (BRS) are demonstrated to be coexistent in the Ag/ZnO/Pt memory device, and both modes are observed to strongly depend on the polarity of forming voltage. The mechanisms of the URS and BRS behaviors could be attributed to the electric-field-induced migration of oxygen vacancies (V_O) and metal-Ag conducting filaments (CFs) respectively, which are confirmed by investigating the temperature dependences of low resistance states in both modes. Furthermore, we compare the resistive switching (RS) characteristics (e.g., forming and switching voltages, reset current and resistance states) between these two modes based on V_O- and Ag-CFs. The BRS mode shows better switching uniformity and lower power than the URS mode. Both of these modes exhibit good RS performances, including good retention, reliable cycling and high-speed switching. The result indicates that the coexistence of URS and BRS behaviors in a single device has great potential applications in future nonvolatile multi-level memory.

Keywords: resistive switching, unipolar, bipolar, oxygen vacancy, metal, conductive filament

PACS: 73.40.Sx, 77.55.hf ,77.22.Jp **DOI:** 10.1088/1674-1056/25/12/127303

1. Introduction

Resistive random access memory (RRAM) has received much attention as a promising candidate for next-generation high-speed, high-density nonvolatile storage technology. The resistive switching (RS) characteristics have been discovered in a variety of inorganic[1–6] and organic[7–10] media, especially in many transition metal oxides such as HfO_2,[11–13] ZrO_2,[14] WO_x,[15] CeO_2,[16] and ZnO.[17–19] The RS mode generally can be classified into unipolar RS (URS) and bipolar RS (BRS) based on whether the switching process depends on voltage polarity. The RS mechanism is generally the formation/rupture of nanoscale conductive filaments (CFs) in the switching layer. The URS mode usually takes place in oxide material,[20] in which the CF is composed of oxygen-vacancies (i.e., V_O) due to the migration of oxygen ions under high electrical field. The Joule heating effect is the main force to induce the rupture of V_O-based CFs, thus the rupture shows no dependence on voltage polarity. For the BRS mode, an active metal CF (e.g., Ag or Cu) forms and ruptures during the set and reset processes corresponding to electrochemical redox reactions.[21] Recently, the behaviors for the URS and BRS coexisting were widely studied due to the possibility to expand the application scope in multi-level memory.[22–25] In addition, it is also interesting to compare the characteristics of V_O-based CFs with those of metal CFs when both of them are formed in a single device, which may be helpful in comprehensively understanding the RS behavior.[26] ZnO material, as one important oxide, is able to exhibit both URS and BRS behaviors.[24,25,27]

In this work, the behaviors for URS and BRS coexisting are demonstrated by utilizing negative and positive forming polarities on the top electrode of Ag/ZnO/Pt cells. The temperature dependences of low resistance states indicate that the CFs consist of V_O defects and Ag atoms in the URS and BRS modes, respectively. Furthermore, the switching characteristics of these two modes are also compared, including forming process, set/reset voltages and high/low resistance states. Both of them can be operated in switching process in a fast speed, which can be regarded as the candidates for next-generation non-volatile memory.

2. Experiments

ZnO-based RRAM devices with active Ag electrodes were fabricated on Pt/Ti/SiO_2/Si substrates as shown in Fig. 1(a). Here, the ZnO film served not only as a switching layer for V_O-CFs, but also as an electrolyte layer for Ag con-

*Project supported by the National Natural Science Foundation of China for Excellent Young Scholars (Grant No. 51422201), the National Natural Science Foundation of China (Grant Nos. 51172041, 51372035, 11304035, 61574031, and 61404026), the National Basic Research Program of China (Grant No. 2012CB933703), the "111" Project, China (Grant No. B13013), the Fund from Jilin Province, China (Grant Nos. 20140520106JH and 20140201008GX), the Research Fund for the Doctoral Program of Higher Education, China (Grant No. 20130043110004), the Fundamental Research Funds for the Central Universities, China (Grant Nos. 2412015KJ008 and 2412016KJ003).

†Corresponding author. E-mail: wangzq752@nenu.edu.cn

‡Corresponding author. E-mail: hyxu@nenu.edu.cn

© 2016 Chinese Physical Society and IOP Publishing Ltd

ductive bridge, which was prepared by sol–gel method: zinc acetate dihydrate was dissolved into 2-methoxyethanol with additional diethanolamine as a stabilizer. A stable and homogeneous solution was obtained after being stirred for 2 h. The ZnO switching layer was fabricated on the Pt bottom electrode by dip-coating method and then calcined at 350 °C for 2 h in air. Finally, metal Ag top-electrodes (TEs) were thermally evaporated and patterned into many circular pads each with a diameter of 0.5 mm using a shadow mask. The ZnO film was characterized by scanning electron microscope (SEM), x-ray diffraction instrument (XRD) and x-ray photoelectron spectroscopy (XPS). The RS properties of the samples were characterized by Keithley 2636A semiconductor analyzer in a voltage-sweep mode. The positive current is defined as the current flowing from the Ag to Pt electrode in the measurements.

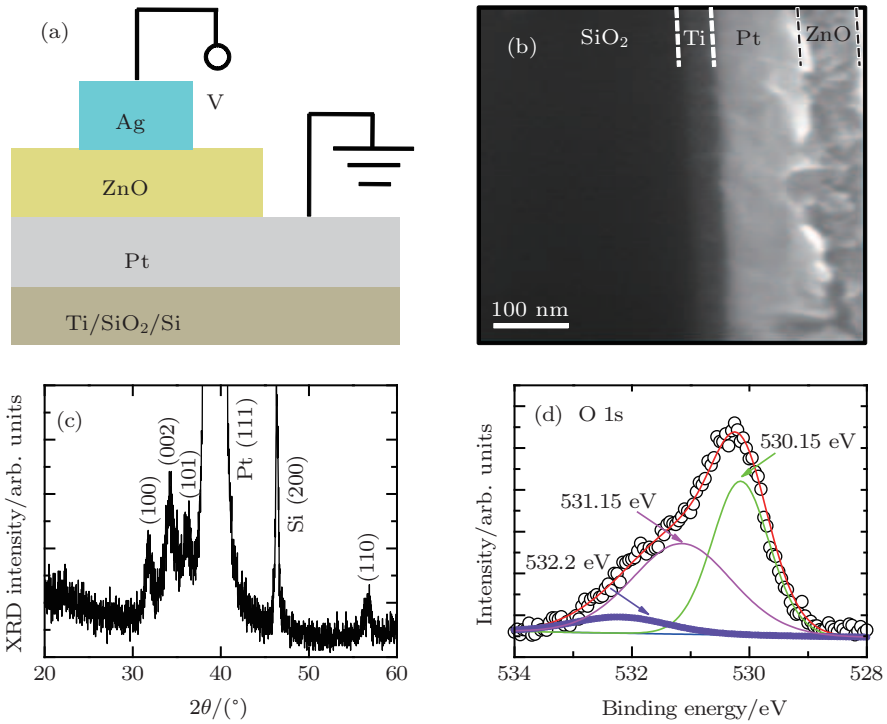


Fig. 1. (color online) (a) Structural diagram of the Ag/ZnO/Pt memory cell. (b) Cross-sectional SEM image of the device. (c) Typical XRD θ–2θ scan data of ZnO thin film grown on Pt (111)/Ti/SiO_2/Si substrate. (d) O 1s core-level XPS spectrum of ZnO layer (open circles), which is deconvoluted into three components (solid lines).

3. Results and discussion

Figure 1(b) shows the cross-sectional SEM image of ZnO thin film, indicating the thickness of thin film is around 85nm. Figure 1(c) shows the typical XRD θ–2θ scan data of ZnO thin film, the diffraction signals display a hexagonal-phase pattern with a highly (002) textured orientation. The XPS analysis is also carried out to investigate the chemical states of O 1s in the ZnO layer as illustrated in Fig. 1(d). By using a Gaussian fitting method, the asymmetric spectra can be divided into three peaks centered nearly at 530.15, 531.15, and 532.20 eV, respectively. As reported in previous work[28] these three peaks are attributed to O^{2-} ions at the intrinsic sites, oxygen vacancies (V_O) and oxygen interstitials (O_i), respectively. This result indicates the existence of non-lattice oxygen (i.e., V_O and O_i) in the ZnO layer.

Current–voltage (I–V) characteristics of devices are studied by direct current (DC) voltage sweep measurements to evaluate the RS memory effect as illustrated in Fig. 2. In order to prevent a permanent dielectric from breaking down, a compliance current of 1 mA is used in the setting process. A forming process is usually required to activate the switching process of RS memory device. Interestingly, different polarities of forming voltage, that is, the positive and negative bias on the Ag TE, can cause different RS behaviors. As shown in Figs. 2(a) and 2(b), a positive forming voltage (V_{F+}) is smaller than the negative one (V_{F-}), and the average values of V_{F+} and V_{F-} are about 1.0 V and −2.8 V respectively, which are obtained by averaging the collecting data from 40 devices. More importantly, the URS and BRS behaviors can be achieved, respectively, (see Figs. 2(c) and 2(d)) after the negative and positive voltage forming process. It is found that the RS parameters and their fluctuation are different between these two modes, including high/low resistance states (HRS and LRS), reset current (I_{reset}) and set/reset voltages (V_{set} and V_{reset}), which will be discussed later. In addition, the difference in forming process and switching modes indicate that the formation and rupture of CFs should be attributed to different RS mechanisms.

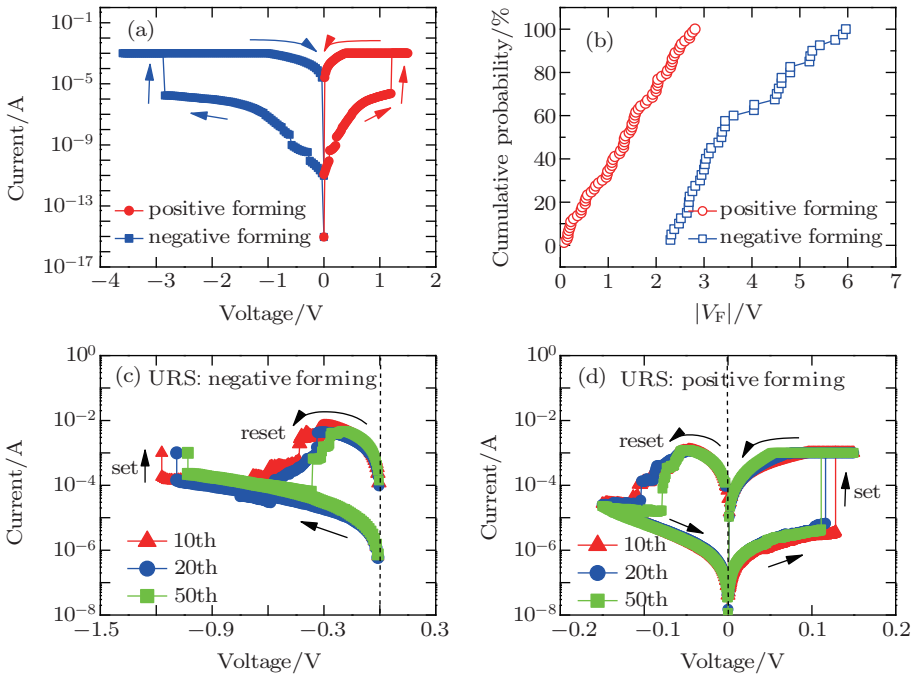


Fig. 2. (color online) Behaviors for URS and BRS coexisting in the single Ag/ZnO/Pt memory cell. (a) Typical positive and negative voltage forming processes for the memory devices. (b) The cumulative distribution of positive and negative forming voltages. (c) and (d) *I*–*V* curve of URS and BRS behaviors after negative and positive forming process.

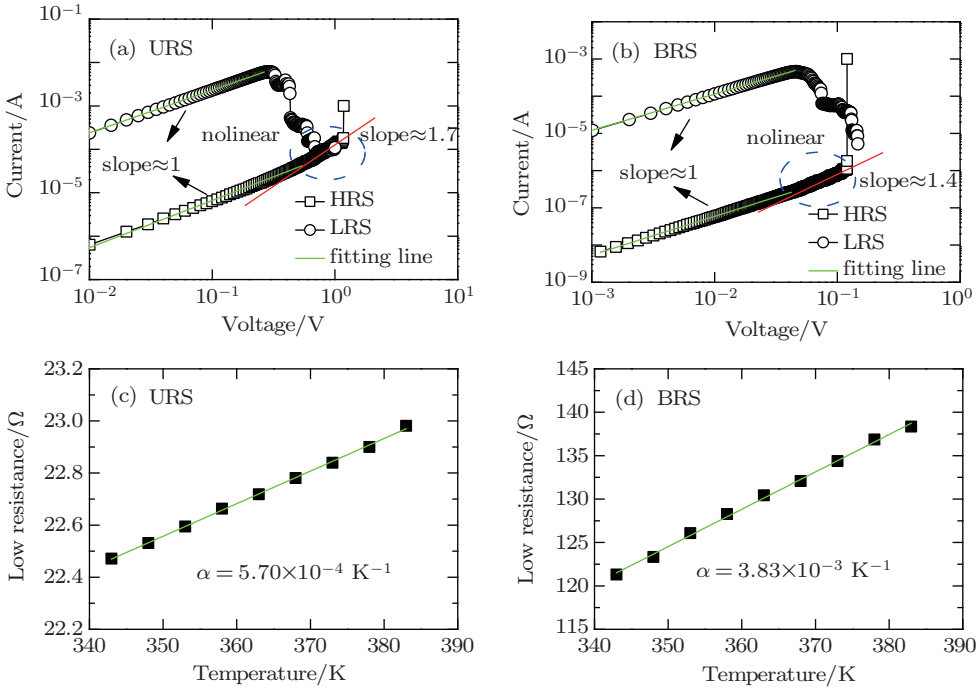


Fig. 3. (color online) Typical *I*–*V* curves of HRS and LRS for (a) URS and (b) BRS modes in log–log scale. (c) and (d) Temperature dependences of LRS state for URS and BRS modes, respectively.

To understand the conduction mechanism, the *I*–*V* curves of URS and BRS are replotted in logarithmic scale as shown in Figs. 3(a) and 3(b). The *I*–*V* characteristics of LRS state display a linearly Ohmic behavior with a slope of 1 for both URS and BRS, indicating the RS behavior can be attributed to the CFs formation/rupture model. For the HRS state, the nonlinear behavior is observed in these two modes. The *I*–*V* curve shows an Ohmic conduction in low-voltage region, but shows a superlinear increase with a slope of ~ 2 in high-voltage region, following Child's law, which is an indication of a trap-controlled space charge limited conduction.[14,16,29] Furthermore, to investigate the RS mechanisms of URS and BRS, the temperature dependences of LRS resistance are investigated in these two modes. As shown in Figs. 3(c) and 3(d), the LRS resistances of both modes linearly increase with temperature rising, showing the metal-like conducting behav-

ior. By choosing T_0 to be 300 K, the linear fits through using the equation $R(T) = R_0[1 + \alpha(T - T_0)]$[20] (where R_0 is the resistance at temperature T_0, and α is the temperature coefficient of resistance) determine α to be 5.70×10^{-4} K^{-1} and 3.83×10^{-3} K^{-1}, respectively. For the URS mode, we note that the temperature coefficients obtained are very close to the values of V_O-based CFs (5.80×10^{-4} K^{-1}),[20] suggesting that the CFs in the current devices are composed of oxygen vacancies. On the other hand, the BRS mode has the α value similar to Ag conductive bridge (4×10^{-3} K^{-1}) reported in defect-free Ag nanowires with a similar size of 30 nm in diameter,[30] thus serving as an identifier of Ag CFs in BRS mode.

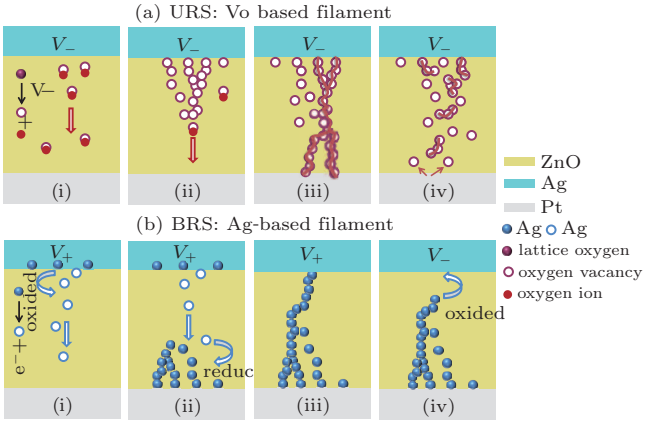


Fig. 4. (color online) Schematic diagrams illustrating the switching mechanism based on (a) V_O filament and (b) Ag filament in the URS and BRS modes.

Based on the above discussion, it is confirmed that the formation and rupture of V_O- based and Ag-based CFs are responsible for the URS and BRS behaviors, respectively. The schematic diagrams for the switching models are illustrated in Figs. 4(a) and 4(b). For URS mode, the electric-field-assisted migration of oxygen ions toward the anode (Fig. 4(a-i)) can induce many V_O defects in the ZnO switching layer (Fig. 4(a-ii)) in the setting process.These V_O defects are connected to each other and form the CFs through ZnO layer (Fig. 4(a-iii)), leading to the resistance state switching from HRS to LRS; in the resetting process, Joule heating can cause the recombination between V_O defects and O^{2-} anions in the weakest region, namely the rupture of CFs (Fig. 4(a-iv)), which is independent of the voltage polarity.[20] For the BRS mode, the species of the mobile ion is cation (Ag^+) instead of oxygen anions, which is the essential difference between V_O-based and Ag-based RRAM. The switching processes of BRS can be interpreted as follows: the anodic dissolution of Ag occurs according to the oxidation reaction $Ag \rightarrow Ag^+ + e^-$ when applying positive voltage to Ag TE, then the Ag^+ migrates across the solid-electrolyte film (Fig. 4(b-i)); the Ag^+ can be reduced to Ag metal under the reduction reaction $Ag^+ + e^- \rightarrow Ag$, resulting in the formation of Ag CFs (Figs. 4(b-ii) and 4(b-iii)); when applying negative voltage to the Ag TE, the reverse oxidation process induces the rupture of Ag CFs (Fig. 4(b-iv)). As illustrated above, the switching process of BRS depends on the voltage polarity on Ag TE. Although the Joule heating may also be conducible to rupturing the Ag CFs in the resetting process in BRS, the critical factor is the reset voltage with opposite polarity to that in the setting process. In summary, the coexistence of URS and BRS of V_O- and Ag-based CFs is obtained in the Ag/ZnO/Pt device by controlling the polarity of forming voltage.

In addition, the V_O-based and metal-based RSs are two important categories in RS memory. Thus, it is also interesting to compare the RS parameters based on these two kinds of CFs in the same device, which is helpful in comprehensively understanding the RS behavior. Since the type of CF strongly depends on the electrode material, the difference in RS parameter can be also regarded as the influence of electrode. Herein, Pt just acts as a conducting electrode in each of URS and BRS due to its inert property, which plays a role similar to Ag in URS. In comparison, the active Ag electrode directly determines the RS characteristics of BRS because of redox reaction of Ag atoms. We observe that the BRS mode (i.e., Ag CFs) has relatively small values of V_F, V_{set}, and V_{reset} than the URS mode (i.e., V_O CFs) as shown in Figs. 2(b) and 5(a). It is known that the oxygen anions and Ag cations need to overcome their barriers for them to migrate and form CFs, and they usually originate from the lattices and Ag electrode. According to previous reports, the potential barrier is much smaller for Ag^+ redox reaction than O^{2-} migration/recombination in ZnO layer.[31] Thus, the smaller V_F and V_{set} of BRS can be attributed to the smaller barrier. On the other hand, Fig. 5(c) shows that both the HRS and LRS of Ag-based CFs are higher than that of V_O-based CFs. For the LRS, besides the compliance current, the Ag-based CFs may also be determined by the limited quantity of adventive Ag^+ from electrode that can migrate into the ZnO layer. However, there is no limitation for the O^{2-} migration from inside. Thus, V_O-based CF has the smaller LRS than Ag-based CF even under the same compliance current, which may also induce much more complex structure. Accordingly, the rupture of V_O-based CF requires higher Joule heating in the resetting process, resulting in larger V_{reset} and I_{reset} as shown in Figs. 5(a) and 5(b). The incomplete rupture may also occur due to the complex structure, which induces residual CFs and lower HRS for URS (Fig. 5(c)). By comparison, a smaller number of Ag atoms in CFs usually induce complete rupture in the resetting process, leaving larger HRS and less remain CFs than those of V_O-based CFs. Furthermore, the variabilities (the ratio of mean value and variance) of V_{set} in BRS and URS are 6.6% and 25.2%, respectively. The same trend can be seen in the I_{reset}, and the variabilities are 10.1% and 53% for Ag-based and V_O-based RRAM. The results indicate that the distribution of Ag-based CFs is smaller and more orderly than that of V_O-based CFs.

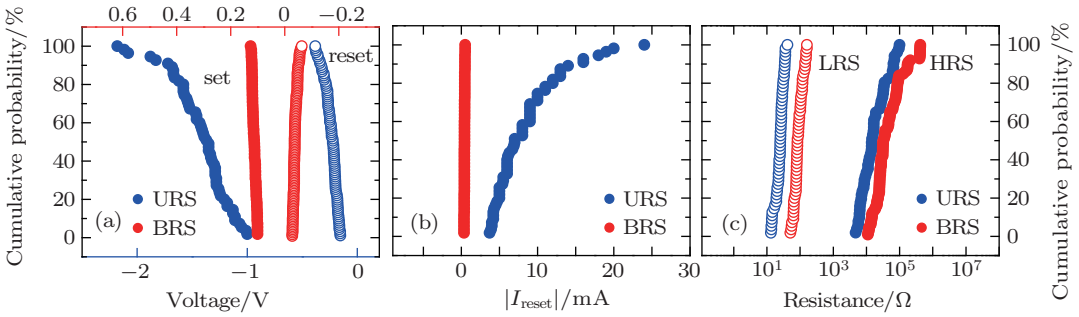


Fig. 5. (color online) Cumulative probabilities of (a) V_{set} and V_{reset}, (b) I_{reset}, and (c) HRS and LRS in the URS and BRS modes, respectively.

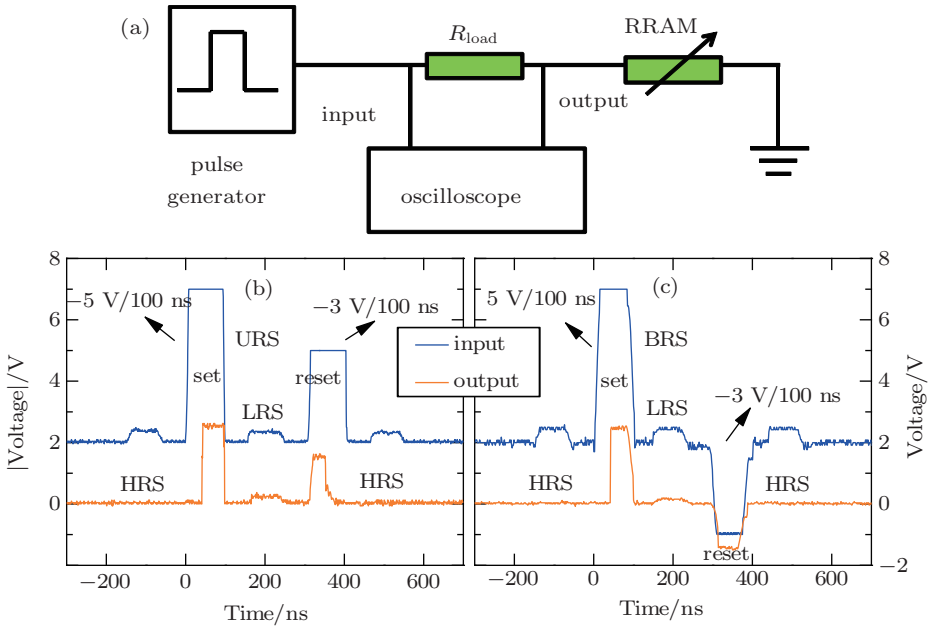


Fig. 6. (color online) (a) Schematic diagram of a setup for high-speed measurement. (b) and (c) Typical switching cycle which is triggered by the setting (±5 V/100) and resetting (−3 V/100 ns) pulses in URS and BRS modes. Here, the resistance states are read using a pulse (0.5 V/100 ns), and the resistance-state transition can be indirectly monitored by the change of output read voltages.

Both the URS and BRS modes of Ag/ZnO/Pt device can present the reliable high-speed switching characteristics as shown in Fig. 6. For high-speed measurement, a setup is needed in which a load resistor (100 Ω) was connected in series to the device as a voltage divider and current limiter.[20] The resistance-state transition in the RRAM device is indirectly monitored by measuring the voltage drop on the load resistor. Figures 6(a) and 6(b) show the switching responses of the device in a setting and resetting cycle triggered by applying ±5 V/100 ns and −3 V/100 ns pulses to URS and BRS, respectively. As shown in Fig. 6, the setting-time and resetting-time are around 40 ns and 80 ns respectively, indicating the capability of current device in high-speed switching. The retention properties of the V_O-based and Ag-based RRAM are also measured to evaluate the non-volatile characteristics of devices. Here, the resistance values of HRS and LRS are read out at 10 mV. As shown in Fig. 7, the resistance states of URS and BRS almost keep constant for longer than 10^4 s at room temperature, indicating the stable non-volatile behaviors of these two modes. Combining with above mentioned properties, we can conclude that both of these modes exhibit great potential applications in future nonvolatile memory.

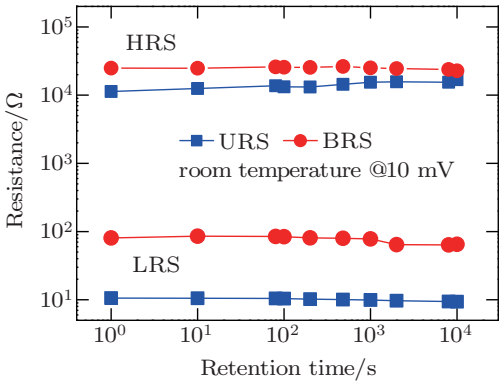


Fig. 7. (color online) Retention characteristics of the URS and BRS modes at room temperature.

4. Conclusions

In this work, we demonstrate the behaviors of URS and BRS coexisting in the single Ag/ZnO/Pt memory device by controlling the polarity of forming process. The study shows that the temperature dependences of LRS, the formation and rupture of V_O-based filament and Ag filament are responsible

for the URS and BRS behaviors. Furthermore, comparison of the switching characteristic between these two modes indicates that the BRS shows less switching fluctuation than the URS, which is attributed to the limited number of Ag^+ cations migrating into the switching layer. Each of URS and BRS exhibits a high switching speed and good retention, suggesting that the Ag/ZnO/Pt memory device has great potential applications in future nonvolatile memory.

References

[1] Waser R and Aono M 2007 *Nat. Mater.* **6** 833
[2] Sun H T, Liu Q, Li C F, Long S B, Lv H B, Bi C, Huo Z L, Li L and Liu M 2014 *Adv. Funct. Mater.* **24** 5679
[3] Wang Z Q, Li X H, Xu H Y, Wang W, Yu H, Zhang X T, Liu Y X and Liu Y C 2010 *J. Phys. D: Appl. Phys.* **43** 385105
[4] Zhang L, Xu H Y, Wang Z Q, Zhao X N, Ma J G and Liu Y C 2014 *J. Phys. D: Appl. Phys.* **47** 455101
[5] Ambrogio S, Balatti S, Choi S and Ielmini D 2014 *Adv. Mater.* **26** 3885
[6] Wu H Y, Zhang J, Zhang Q L, Yang H and Luo J K 2014 *Chin. Phys. Lett.* **31** 057305
[7] Song S, Cho B, Kim T, Ji Y, Jo M, Wang G, Choe M, Kahng Y H, Hwang H and Lee T 2010 *Adv. Mater.* **22** 5048
[8] Hosseini N R and Lee J S 2015 *ACS Nano* **9** 419
[9] Cho B, Yun J M, Song S, Ji Y, Kim D Y and Lee T 2011 *Adv. Funct. Mater.* **21** 3976
[10] Song Y, Jang J, Yoo D, Jung S H, Hong S, Lee J K and Lee T 2015 *Organic Electronics* **17** 192
[11] Pang H and Deng N 2014 *Chin. Phys. Lett.* **31** 107303
[12] Tan T T, Chen X, Guo T T and Liu Z T 2013 *Chin. Phys. Lett.* **30** 107302
[13] Jiang R, Du X H, Han Z Y and Sun W D 2015 *Acta Phys. Sin.* **64** 207302 (in Chinese)
[14] Lei X Y, Liu H X, Gao H X, Yang H N, Wang G M, Long S B, Ma X H and Liu M 2014 *Chin. Phys. B* **23** 117305
[15] Wu H Q, Wu M H, Li X Y, Bai Y, Deng N, Yu Z P and Qian H 2015 *Chin. Phys. B* **24** 058501
[16] Ismail M, Abbas M W, Rana A M, Talib I, Ahmed E, Nadeem M Y, Tsai T L, Chand U, Shah N A, Hussain M, Aziz A and Bhatti M T 2014 *Chin. Phys. B* **23** 126101
[17] Chuang M Y, Chen Y C, Su Y K, Hsiao C H, Huang C S, Tsai J J and Yu H C 2014 *ACS Appl. Mater. Interf.* **6** 5432
[18] Dongale T D, Khot K V, Mali S S, Patil P S, Gaikwad P K, Kamat R K and Bhosale P N 2015 *Mater. Sci. Semicond. Process.* **40** 523
[19] Zhao J, Dong J Y, Ren S X, Zhang L Y, Zhao X and Chen W 2014 *Chin. Phys. B* **23** 127301
[20] Wang Z Q, Xu H Y, Zhang L, Li X H, Ma J G, Zhang X T and Liu Y C 2013 *Nanoscale* **5** 4490
[21] Zhao X N, Xu H Y, Wang Z Q, Zhang L, Ma J G and Liu Y C 2015 *Carbon* **91** 38
[22] Xu D L, Xiong Y, Tang M H, Zeng B W, Xiao Y G and Wang Z P 2013 *Chin. Phys. B* **22** 117314
[23] Hu W, Chen X M, Wu G H, Lin Y T, Qin N and Bao D H 2012 *Appl. Phys. Lett.* **101** 063501
[24] Xu D L, Xiong Y, Tang M H and Zeng B W 2014 *J. Alloys Compd.* **584** 269
[25] Lee S, Kim H, Park J and Yong K 2010 *J. Appl. Phys.* **108** 076101
[26] Calderoni A, Sills S and Ramaswamy N 2014 *IEEE IMW Tech. Dig.* pp. 1–4
[27] Yang Y C, Pan F, Liu Q, Liu M and Zeng F 2009 *Nano Lett.* **9** 1636
[28] Fan H B, Yang S Y, Zhang P F, Wei H Y, Liu X L, Jiao C M, Zhu Q S, Chen Y H and Wang Z G 2007 *Chin. Phys. Lett.* **24** 2108
[29] Liang K D, Huang C H, Lai C C, Huang J S, Tsai H W, Wang Y C, Shih Y C, Chang M T, Lo S C and Chueh Y L 2014 *ACS Appl. Mater. Interf.* **6** 16537
[30] Bid A, Bora A and Raychaudhuri A K 2006 *Phys. Rev. B* **74** 035426
[31] Xue W H, Xiao W, Shang J, Chen X X, Zhu X J, Pan L, Tan H W, Zhang W B, Ji Z H, Liu G, Xu X H, Ding J and Li R W 2014 *Nanotechnology* **25** 425204